

# On the Non-existence of a Sharp Cooling Break in GRB Afterglow Spectra

Z. Lucas Uhm<sup>1,2</sup>, Bing Zhang<sup>1,3,2</sup>

## ABSTRACT

Although the widely-used analytical afterglow model of gamma-ray bursts (GRBs) predicts a sharp cooling break  $\nu_c$  in its afterglow spectrum, the GRB observations so far rarely show clear evidence for a cooling break in their spectra or its corresponding temporal break in their light curves. Employing a Lagrangian description of the blast wave, we conduct a sophisticated calculation of the afterglow emission. We precisely follow the cooling history of non-thermal electrons accelerated into each Lagrangian shell. We show that a detailed calculation of afterglow spectra does not in fact give rise to a sharp cooling break at  $\nu_c$ . Instead, it displays a very mild and smooth transition, which occurs gradually over a few orders of magnitude in energy or frequency. The main source of this slow transition is that different mini-shells have different evolution histories of the comoving magnetic field strength  $B$ , so that deriving the current value of  $\nu_c$  of each mini-shell requires an integration of its cooling rate over the time elapsed since its creation. We present the time evolution of optical and X-ray spectral indices to demonstrate the slow transition of spectral regimes, and discuss the implications of our result in interpreting GRB afterglow data.

*Subject headings:* gamma-ray burst: general — radiation mechanisms: non-thermal — shock waves

## 1. Introduction

The broad-band afterglow emission of gamma-ray bursts (GRBs) (Costa et al. 1997; van Paradijs et al. 1997), has been interpreted as synchrotron radiation from a relativistic blast wave, which sweeps up a surrounding ambient medium (Mészáros & Rees 1997;

---

<sup>1</sup>Kavli Institute for Astronomy and Astrophysics, Peking University, Beijing 100871, China

<sup>2</sup>Department of Physics and Astronomy, University of Nevada, Las Vegas, NV 89154, USA; uhm@physics.unlv.edu, zhang@physics.unlv.edu

<sup>3</sup>Department of Astronomy, Peking University, Beijing 100871, China

Sari et al. 1998). This widely-used analytical model of GRB afterglows (Sari et al. 1998) predicts a sharp cooling break at  $\nu_c$  in their spectra, determined by synchrotron cooling rate of non-thermal electrons during the dynamical time scale of the relativistic blast wave.

GRB afterglow observations so far rarely show clear evidence for a cooling break in their spectra or its corresponding temporal break in light curves with a spectral index change across the break. The Swift satellite (Gehrels et al. 2004) has accumulated 9 years of afterglow data. In the X-ray band where  $\nu_c$  likely shows up, usually one or two steepening breaks are observed in the canonical X-ray light curves (Zhang et al. 2006; Nousek et al. 2006). However, the change of decay slope is inconsistent with  $\nu_c$  crossing, and more importantly, there is essentially no spectral index change across the temporal breaks (e.g. Liang et al. 2007, 2008). Inferences of  $\nu_c$  were only occasionally drawn in rare bursts (e.g. Filgas et al. 2011). The missing  $\nu_c$  in individual GRBs may be understood as that the shock parameters are such that  $\nu_c$  lies in between optical and X-ray bands, so that there is no  $\nu_c$  crossing during the observational time (e.g. Curran et al. 2010; Oates et al. 2011). However, the lack of  $\nu_c$  in almost entire Swift afterglow data set suggests that this must be an effect intrinsic to GRB physics.

The simple analytical model (Sari et al. 1998) assumes that the entire postshock material forms a single zone with the same energy density and magnetic field. The single shocked zone is endowed with a broken power-law electron energy distribution with a break at a “cooling” Lorentz factor  $\gamma_c$ . Granot & Sari (2002) relaxed this assumption and introduced other factors such as the Blandford-McKee (BM) solution (Blandford & McKee 1976), the curvature effect, and adiabatic cooling to describe the shocked electrons, and showed that the shape of spectral breaks is much smoother than predicted by the analytical model (see also van Eerten & Wijers (2009); Leventis et al. (2012)). However, since their model introduces many factors, one could not identify the main source of smoothing.

In this paper, we perform a detailed study on the formation of GRB afterglow spectra, by adopting a Lagrangian description of the shocked region (Uhm et al. 2012, hereafter U12). We obtain a very smooth cooling break  $\nu_c$  in the afterglow spectrum. We identify its main physical origin, and show that a smooth  $\nu_c$  is ubiquitous and intrinsic to a wide range of astrophysical phenomena involving synchrotron cooling.

## 2. Smooth cooling break and its physical origin

Following Uhm (2011) and U12 (Section 2), we make use of a semi-analytic formulation of a relativistic blast wave in order to find its dynamics accurately from an initial coasting

phase through a deceleration stage. Then, as described in U12 (Section 3), we adopt a Lagrangian description of the blast wave to conduct a sophisticated calculation of its afterglow emission. The blast is viewed as being made of many different Lagrangian shells  $\{\delta m^i\}$ . Here the index  $i$  is used to denote each Lagrangian shell. We keep track of an adiabatic evolution of each shell  $\delta m^i$  to find a time evolution of the magnetic field  $B^i$  of the shell (U12, Section 3.1). The cooling history of an electron spectrum is also followed individually for every shell  $\delta m^i$  (U12, Section 3.2).

Radiative and adiabatic cooling of an electron with the Lorentz factor  $\gamma_e$  is described by the first and second term below, respectively, (U12, Equation (17))

$$\frac{d}{dt'} \left( \frac{1}{\gamma_e} \right) = \frac{\sigma_T}{6\pi m_e c} B^{i2} - \frac{1}{4} \left( \frac{1}{\gamma_e} \right) \frac{d \ln p^i}{dt'}. \quad (1)$$

Here  $t'$  is the time measured in the co-moving fluid frame,  $\sigma_T$  is the Thomson cross section,  $m_e$  is the electron mass,  $c$  is the speed of light, and  $B^i$  and  $p^i$  are respectively the magnetic field and the pressure of the shell  $\delta m^i$  where the electron sits in. The Compton parameter  $Y$  that describes a contribution of inverse Compton scattering to the cooling rate of electrons is omitted here. We assume that electrons are accelerated into a power-law distribution of slope  $p$  above an injection Lorentz factor  $\gamma_{\text{inj}}$  in a fresh shell  $\delta m^i$  at a shock front (forward shock (FS) or reverse shock (RS)). As the blast wave propagates, the electron spectrum in the shell  $\delta m^i$  evolves in time. All the electrons inside the spectrum cool down, and their cooling history is governed by the differential Equation (1). Thus, we use Equation (1) to find a time evolution of a minimum Lorentz factor  $\gamma_m^i$  and a cooling Lorentz factor  $\gamma_c^i$  for the shell  $\delta m^i$ . For simplicity, we further assume that the shell  $\delta m^i$  maintains a power-law electron spectrum of slope  $p$ , bounded by two Lorentz factors  $\gamma_m^i$  and  $\gamma_c^i$ , as time goes.

More explicitly, when the shell  $\delta m^i$  is created at a shock front (FS or RS) at the co-moving time  $t'_i$ , the electron spectrum injected into the shell  $\delta m^i$  has the initial Lorentz factors

$$\gamma_m^i(t'_i) = \gamma_{\text{inj}}(t'_i), \quad \gamma_c^i(t'_i) = +\infty, \quad (2)$$

where

$$\gamma_{\text{inj}}(t') = 1 + \frac{p-2}{p-1} \frac{m_p}{m_e} \epsilon_e [\bar{\gamma}_p(t') - 1]. \quad (3)$$

Here,  $m_p$  is the proton mass, and  $\bar{\gamma}_p(t')$  is the mean Lorentz factor of protons in the fresh shell created at the shock front at co-moving time  $t'$ . Then, the Lorentz factors  $\gamma_m^i(t'_j)$  and  $\gamma_c^i(t'_j)$  of the shell  $\delta m^i$  at a later time  $t'_j$  ( $> t'_i$ ) can be found by integrating Equation (1) from  $t'_i$  to  $t'_j$ .<sup>1</sup>

---

<sup>1</sup> With initial values given by Equation (2),  $\gamma_m^i(t'_j) < \gamma_c^i(t'_j)$  is always expected for the given shell  $\delta m^i$ .

We take the following simple fiducial example to calculate the afterglow spectra. (1) A constant density  $\rho_1(r)/m_p = n_1(r) = 1 \text{ cm}^{-3}$  is assumed for the ambient medium. (2) The ejecta has a constant kinetic luminosity  $L_{\text{ej}}(\tau) = L_0 = 10^{52} \text{ erg/s}$  for a duration of  $\tau_b = 5 \text{ s}$ , so that the total isotropic energy of the burst is  $E_b = L_0 \tau_b = 5 \times 10^{52} \text{ erg}$ . (3) The ejecta is assumed to emerge with a constant Lorentz factor  $\Gamma_{\text{ej}} = 300$ , so that the RS is short-lived. (4) The burst is assumed to be located at a redshift  $z = 1$ . As in U12 (Equation (35)), a flat  $\Lambda$ CDM universe is adopted for the luminosity distance, with the parameters  $H_0 = 71 \text{ km s}^{-1} \text{ Mpc}^{-1}$ ,  $\Omega_m = 0.27$ , and  $\Omega_\Lambda = 0.73$  (the concordance model). (5) The microphysics parameters are adopted as  $p = 2.3$ ,  $\epsilon_e = 10^{-1}$ , and  $\epsilon_B = 10^{-3}$  (for slow cooling) or  $10^{-1}$  (for fast cooling). In the following, we perform calculations under the assumptions of two different pressure profiles across the blast wave: a constant profile (§2.1) and a Blandford-McKee (BM) profile (§2.2).

## 2.1. Constant profile of pressure

We find the blast wave dynamics of the fiducial example above, by making use of Uhm (2011) and U12 (Section 2). It is found that the RS is short-lived, as expected, vanishing at around  $t_{\text{obs}} = 20 \text{ s}$ . Once the RS has crossed the ejecta, the blast wave deceleration transitions to and then agrees with the BM solution. During the transition phase, the deceleration (viewed as a function of radius  $r$ ) is slightly slower than the BM solution,<sup>2</sup> since the pressure profile is being lowered into the BM profile and thermal (internal) energy contained there is being adiabatically converted into kinetic bulk motion. As the RS is short-lived here, we focus on the FS afterglow spectra from the FS shocked region (i.e., region 2). The magnetic field  $B^i(t')$  of  $\delta m^i$  at any co-moving time  $t'$  ( $t'_i < t' < t'_j$ ) is found following U12 (Section 3.1) while assuming, for simplicity, a constant profile of pressure over region 2, i.e.,  $p^i(t') = p_f(t')$  for all shocked shells  $\{\delta m^i\}$  in region 2 at every co-moving time  $t'$ . Here,  $p_f$  is the pressure at the FS front. Integrating Equation (1) from  $t'_i$  to  $t'_j$  with the initial values at  $t'_i$  (Equation (2)), we obtain the Lorentz factors  $\gamma_m^i(t'_j)$  and  $\gamma_c^i(t'_j)$  of each shell  $\delta m^i$  at time  $t'_j$ .

Taking also into account the equal-arrival-time “curvature effect” of spherical shells, the

---

However,  $\gamma_c^i(t'_j) < \gamma_m^i(t'_j)$  can also happen for fast cooling, which corresponds to the fast cooling regime ( $\gamma_c < \gamma_m$ ) in the context of Sari et al. (1998).

<sup>2</sup>This implies that, during the transition phase, the blast wave deceleration (now viewed as a function of observer time  $t_{\text{obs}}$ ) is slightly faster than the BM case. For this reason, in Figure 3 below, the separation between two injection breaks at  $10^2 \text{ s}$  and  $10^3 \text{ s}$  is slightly wider than that expected from the BM deceleration.

Doppler boosting of radial bulk motion, and different radii  $\{r^i\}$  of individual shells (U12, Section 3.3), we calculate the FS afterglow spectra for the fiducial example above. The result is shown in Figure 1. For panels (a) and (b), we use  $\epsilon_B = 10^{-3}$  (slow cooling), and for panels (c) and (d), we use  $\epsilon_B = 10^{-1}$  (fast cooling). The upper panels (a) and (c) show the instantaneous afterglow spectra at observer times  $t_{\text{obs}} = 10^1, 10^2, 10^3, 10^4$ , and  $10^5$  s, and the lower panels (b) and (d) show a time evolution of spectral indices  $\beta$  (with a convention,  $F_\nu \propto \nu^{-\beta}$ ) at 1 keV and  $R$  band. As shown in panel (a), the afterglow spectra displays a very mild and smooth transition over a few orders of magnitude in frequency or energy in the vicinity of a cooling break. In particular, the spectral indices shown in panel (b) highlight that a transition from  $\beta = (p - 1)/2$  spectral regime to  $\beta = p/2$  segment is very slow and takes several orders of magnitude in observer time  $t_{\text{obs}}$ . The outcome in panels (c) and (d) (fast cooling) is even more interesting. An expected transition from  $\beta = -1/3$  to  $\beta = 1/2$  is not present. The characteristic spectral segment with  $\beta = 1/2$  is not even reproduced. Instead, an almost flat ( $\beta \approx 0$ ) spectral segment is observed at around the optical bands.

In an effort of identifying the main source of this smoothness, we first remove the curvature effect and place all the shocked shells at the same radius  $r_f$  where the FS is located. All other steps of the calculations remain the same as above. We find the afterglow spectra again for the fiducial example, and show the result in Figure 2. As shown in panel (a), the injection break  $\nu_m$  is now sharper than in Figure 1, which can also be seen in panel (b) by noticing that the transition from  $\beta = -1/3$  to  $\beta = (p - 1)/2$  regime is faster than in Figure 1. The injection break  $\nu_m$  in panels (c) and (d) (fast cooling) is also more visible than in Figure 1; panel (d) exhibits a sharper feature between  $\beta = 1/2$  regime and  $\beta = p/2$  regime. However, the afterglow spectra in panel (a) still exhibit a very mild and smooth cooling break. The spectral indices in panel (b) show that the transition from  $\beta = (p - 1)/2$  to  $\beta = p/2$  segment is just as slow as in Figure 1 and still takes several orders of magnitude in observer time  $t_{\text{obs}}$ . Thus, this is also an indication that the curvature effect is nearly negligible in smoothing out a break if the break is already sufficiently smooth.

For panels (c) and (d) (fast cooling), the expected transition from  $\beta = -1/3$  to  $\beta = 1/2$  regime is not present again; the characteristic fast-cooling segment with  $\beta = 1/2$  is not reproduced. The nearly flat ( $\beta \approx 0$ ) spectral segment at around the optical bands is now more visible than in Figure 1. This is because the standard fast-cooling synchrotron spectrum with index  $\beta = 1/2$  below the injection frequency (Sari et al. 1998), which has been widely believed, is not valid for a general problem involving a non-steady state electron spectrum of the emitting region, which we recently showed in the context of GRB prompt emission (Uhm & Zhang 2013). Briefly speaking, the standard fast cooling spectrum is valid only for a steady state electron distribution, which may be achieved when a constant strength of magnetic field is invoked for the emitting region. However, in a rapidly expanding source

such as for GRB prompt emission, the magnetic field strength in the emitting region cannot be preserved as a constant. The same is also true for GRB afterglow radiation, since the blast wave is decelerating. Uhm & Zhang (2013) showed that, for such a system with a decreasing magnetic field in the region, the fast cooling electron distribution is not in a steady state, forming a significantly harder spectrum than the standard one. The resulting synchrotron photon spectrum is also significantly harder than the standard one with  $\beta = 1/2$ , naturally yielding a nearly flat ( $\beta \approx 0$ ) spectral segment below the injection frequency. A more detailed investigation regarding this fast cooling spectrum in the context of GRB afterglow emission will be presented in a different paper.

Since the curvature effect is not the main source of smoothing the cooling break, the next source we suspect is the adiabatic cooling term included in Equation (1). Dropping out this term from Equation (1) and integrating it from  $t'_i$  to  $t'_j$ , we get

$$\frac{1}{\gamma_c^i(t'_j)} = \frac{\sigma_T}{6\pi m_e c} \int_{t'_i}^{t'_j} [B^i(t')]^2 dt', \quad (4)$$

for  $\gamma_c^i(t'_j)$  at time  $t'_j$ , since  $\gamma_c^i(t'_i) = +\infty$ . For the same fiducial example, we calculate the afterglow spectra while making use of Equation (4) instead of Equation (1) in the calculation of  $\gamma_c^i(t'_j)$ . The resulting afterglow spectra are not very different from those shown in Figure 2. Thus, the adiabatic cooling term in Equation (1) is not the main source of this slow transition through the cooling break.

The analytical method of Sari et al. (1998) uses the instantaneous  $B$  to estimate the cooling time scale, which implicitly assumes that the magnetic field strength  $B$  did not evolve during the dynamical evolution of the blast wave. To check whether this is the main source of discrepancy, we take the  $B^2$  term out of the integration in Equation (4). Using its current value  $B^i(t'_j)$  at time  $t'_j$ , we get

$$\frac{1}{\gamma_c^i(t'_j)} = \frac{\sigma_T}{6\pi m_e c} [B^i(t'_j)]^2 (t'_j - t'_i), \quad (5)$$

which resembles the widely used expression for  $\gamma_c$  of Sari et al. (1998), their Equation (6). Employing Equation (5) in the calculation of  $\gamma_c^i(t'_j)$  and, for simplicity, adopting  $\gamma_m^i(t'_j) = \gamma_{\text{inj}}(t'_j)$  (Equation (3)) in all shocked shells  $\{\delta m^i\}$ , we find the FS afterglow spectra for the fiducial example. The result is shown in Figure 3. Panel (a) now displays a considerably sharp cooling break. Thus, using Equation (5) and based on the Lagrangian description of the blast wave, we closely reproduce the analytical afterglow spectra shown in Sari et al. (1998). On the other hand, panels (c) and (d) (fast cooling) indicate that the predicted spectral segment with  $\beta = 1/2$  is still not recovered. Uhm & Zhang (2013), in particular, our Model [a] there, reproduced the standard fast cooling spectrum with  $\beta = 1/2$ , (i) by

assuming a constant strength of magnetic field  $B$  in the emitting region, (ii) by adopting a constant injection rate  $R_{\text{inj}}$  of accelerated electrons, and (iii) by essentially following cooling of all the electrons inside the spectrum individually. Here (i) and (ii) are to assure that the global electron spectrum of the emitting region remains in a steady-state, and (iii) is to accurately follow a time evolution of the entire electron spectrum shape in each injection shell. Equation (5) would play a similar role as (i) does, since  $B$  is taken out of the time integration. However, for this afterglow calculation, we do not keep a constant injection rate  $R_{\text{inj}}$ , since it is determined by the blast wave dynamics. Also, as mentioned earlier, we do not follow cooling of all the electrons inside the spectrum. For simplicity, we only follow the time evolution of two Lorentz factors  $\gamma_m^i$  and  $\gamma_c^i$  for each shell  $\delta m^i$ , and then assume that the shell  $\delta m^i$  maintains a power-law distribution of slope  $p$  between  $\gamma_m^i$  and  $\gamma_c^i$ . These two issues (ii) and (iii) would become potential reasons why the standard spectral segment  $\beta = 1/2$  is not fully recovered here. This will be further investigated in a different paper.

Thus, we have identified the main source of the smooth cooling break. The approach made above to get Equation (5) from Equation (4) cannot be justified, since the magnetic field strength  $B^i$  in the shell  $\delta m^i$  must be a time-dependent quantity. This requires an integration of  $B^{i2}$  over time in order to correctly follow the cooling history of electrons in the shell  $\delta m^i$ , as is described by Equation (4).

## 2.2. BM profile of pressure and Lorentz factor

After the RS crosses the ejecta, it is expected that the blast wave would be adjusted to the Blandford-McKee (1976) self-similar profile (Kobayashi & Sari 2000). Granot & Sari (2002) also obtained smooth spectral breaks in their detailed numerical modeling. Their model invokes the evolution of magnetic fields in the emission region, curvature effect, and the BM density/Lorentz factor profile of the blast wave. In order to investigate the effect of BM profiles on the shape of afterglow spectra, we now take into account the BM profiles in our numerical calculations. The fiducial example above has a short-lived RS. Thus, once the RS crosses the end of the ejecta, we fully adopt the BM profiles in our numerical code.

For a power-law profile of the ambient medium density,  $\rho_1(r)/m_p = n_1(r) \propto r^{-k}$ , when the FS front is located at radius  $r_f$  with the Lorentz factor  $\Gamma_f$ , a shocked fluid element at radius  $r^i$  ( $\leq r_f$ ) is described by the BM solution (Blandford & McKee 1976) as follows,

$$p = \frac{2}{3} \rho_1(r_f) c^2 \Gamma_f^2 \chi^{-\frac{17-4k}{3(4-k)}}, \quad (6)$$

$$\gamma = \frac{1}{\sqrt{2}} \Gamma_f \chi^{-\frac{1}{2}}, \quad (7)$$

$$n = 2\sqrt{2} n_1(r_f) \Gamma_f \chi^{-\frac{10-3k}{2(4-k)}}, \quad (8)$$

where the coordinate  $\chi$  of the fluid element is given by

$$\chi = 1 + 2(4-k) \Gamma_f^2 (1 - r^i/r_f). \quad (9)$$

The fluid element has pressure  $p$  and number density  $n$  in the co-moving frame and moves with the Lorentz factor  $\gamma$  in the lab frame. For an adiabatic blast wave, this fluid element flows adiabatically and should satisfy  $p \propto n^{4/3}$ . Also, the FS front satisfies  $\Gamma_f^2 \propto r_f^{k-3}$  if the blast wave is adiabatic. Then, together with Equations (6) and (8), the relation  $p \propto n^{4/3}$  results in a simple and useful relationship  $\chi \propto r_f^{4-k}$  (see also Granot & Sari (2002)). In connection with our Lagrangian description of the blast wave, when a shell  $\delta m^i$  is created at the FS front at lab time  $t_i$ , the  $\chi^i$  coordinate of  $\delta m^i$  at time  $t_i$  is  $\chi^i(t_i) = 1$  since its radius is equal to the FS radius  $r_f(t_i) \equiv r_f^i$ . Then, the  $\chi^i$  coordinate of the shell  $\delta m^i$  at a later lab time  $t (\geq t_i)$  is given by

$$\chi^i(t) = \left[ \frac{r_f(t)}{r_f^i} \right]^{4-k}. \quad (10)$$

Using Equations (9) and (10), we then find the radius  $r^i$  of  $\delta m^i$  at time  $t (\geq t_i)$  as

$$r^i(t) = r_f(t) \left[ 1 - \frac{\chi^i(t) - 1}{2(4-k) \Gamma_f^2(t)} \right], \quad (11)$$

where  $\Gamma_f(t)$  is the FS Lorentz factor at time  $t$ . Also, Equations (6) and (7) give the pressure  $p^i(t)$  and the Lorentz factor  $\gamma^i(t)$  of the shell  $\delta m^i$  at time  $t (\geq t_i)$ , respectively,

$$p^i(t) = p_f(t) [\chi^i(t)]^{-\frac{17-4k}{3(4-k)}}, \quad (12)$$

$$\gamma^i(t) = \frac{1}{\sqrt{2}} \Gamma_f(t) [\chi^i(t)]^{-\frac{1}{2}}. \quad (13)$$

The fiducial example has  $k = 0$  (a constant density medium). Adopting the BM profiles described above, we calculate the afterglow spectra again for the fiducial example. First, we find the magnetic field  $B^i(t)$  of the shell  $\delta m^i$  at time  $t (\geq t_i)$  following U12 (Section 3.1) but using the BM pressure profile (Equation (12)) rather than the constant profile of pressure. Second, as we did in Figure 1, we fully include the curvature effect (spherical curvature of shells, the Doppler boosting of radial motion, and different radii of shells). Equation (11) gives the radii of shells for the BM profile. Also, due to the BM Lorentz factor profile (Equation (13)), each shell has its own Doppler boosting factor. Thus, we accordingly modify the synchrotron photon frequency and spectral flux density that are emitted from the shell. Third, we use Equation (1) to correctly follow cooling of electrons. The co-moving clock  $t'$



in a shell flows now differently from clocks in other shells. Taking this effect into account, we integrate Equation (1) from  $t_i$  to  $t_j$  ( $> t_i$ ) with the initial values at  $t_i$  (Equation (2)) and obtain the Lorentz factors  $\gamma_m^i$  and  $\gamma_c^i$  for the shell  $\delta m^i$  at time  $t_j$ .

The resulting afterglow spectra is shown in Figure 4. As shown in panel (a), the spectra still exhibit a very mild and smooth cooling break  $\nu_c$ . The spectral indices in panel (b) show that the transition from  $\beta = (p - 1)/2$  regime to  $\beta = p/2$  segment is still as slow as in Figure 1 (constant profile of pressure), but occurs later than in Figure 1 indicating that the cooling break is located at higher energy than in Figure 1. The outcome in panels (c) and (d) (fast cooling) is similar to that of Figure 1, except that the flat ( $\beta \approx 0$ ) spectral segment at around the optical bands is less prominent than in Figure 1. For comparison, we show these two results together in Figure 5: solid line for spectra from Figure 4 (BM profile) and dotted line for spectra from Figure 1 (constant profile). The left panel is for  $\epsilon_B = 10^{-3}$  (slow cooling), and the right panel is for  $\epsilon_B = 10^{-1}$  (fast cooling). This fiducial example has a short-lived RS, which vanishes at around  $t_{\text{obs}} = 20$  s. Therefore, two results are identical to each other at  $t_{\text{obs}} = 10$  s. For the spectra after the RS is vanished, the general trend is that the dotted lines have higher spectral flux  $F_\nu$  than the solid lines, because the blast wave with a constant profile of pressure has higher energy density and magnetic field than the blast wave with a BM profile of pressure. However, the difference in spectral flux  $F_\nu$  becomes less significant as we go to higher photon frequency  $\nu_{\text{obs}}$ . This is because only recently shocked fresh shells have electrons with higher energy, which could contribute to higher frequency range of spectra. As for these fresher shells, the difference between two profiles becomes less significant. In particular, for the right panel (fast cooling), two results are essentially identical to each other at high frequency, indicating that only very fresh shells contribute to this energy range. For the left panel (slow cooling), the dotted lines have an injection break at higher frequency than the solid lines, because the dotted lines with constant pressure profile underestimate the degree of adiabatic cooling of electrons when compared to the solid lines with the BM profile; see the adiabatic cooling term in Equation (1). Also, from the left panel (slow cooling), one may notice that the solid lines have a cooling break at higher frequency than the dotted lines, as mentioned above. This is because the dotted lines have higher magnetic field (namely, higher rate of radiative cooling of electrons) than the solid lines. Nevertheless, the smoothness of cooling break in two results is comparable to each other (also shown in panel (b) of Figure 4). This again suggests that the magnetic field evolution effect is the main physical origin for the smooth cooling breaks.

### 3. Conclusions and Discussion

In this paper, we perform a detailed study on the formation of GRB afterglow spectra, by adopting a Lagrangian description of the shocked region following Uhm et al. (2012). We precisely follow the cooling history of the electron spectrum for each individual Lagrangian shell, and integrate over all shells to find the instantaneous flux spectra. We show that this detailed calculation gives rise to a very mild and smooth cooling break, which occurs gradually over a few orders of magnitude in energy. We identify the main source of this slow transition as due to the different  $B$  evolution histories of different mini shells. This gives rise to an additional spreading of  $\nu_c$  for different shells, aside from the simple age difference ( $t'_j - t'_i$ ). This extra spreading is the main source of the smooth  $\nu_c$ .

We have shown that this effect exists regardless of whether the curvature effect of a relativistic spherical shell is taken into account. It does not depend on the details of the blast wave dynamics or whether it is FS or RS. In fact, it is an intrinsic effect relevant to a wide range of astrophysical phenomena that invokes synchrotron cooling of electrons.

It is interesting to note that the injection break  $\nu_m$  is always much sharper than  $\nu_c$  for slow cooling, and is usually so for fast cooling, even though it becomes somewhat smoother when the curvature effect is taken into account. If a sharp spectral break is observed in an astrophysical phenomenon, this break is very likely an injection break, and cannot be a cooling break.

Simple analytical GRB afterglow models predict some “closure relations” between the temporal decay index  $\alpha$  and the spectral index  $\beta$  (e.g. Mészáros & Rees 1997; Sari et al. 1998, 1999; Chevalier & Li 2000; Dai & Cheng 2001; Zhang & Mészáros 2004; Gao et al. 2013). These models have been applied to the Swift XRT data (from which both temporal decay index and spectral index can be extracted) to test the validity of the afterglow models (e.g. Liang et al. 2007, 2008; Panaitescu 2007; Willingale et al. 2007; Evans et al. 2009). The result of this paper suggests that the analytical closure relation above  $\nu_c$  is usually not achieved. The data could still be consistent with the afterglow theory even if the data fall into the grey zone between the analytical  $\nu < \nu_c$  and  $\nu > \nu_c$  closure relation lines in the  $\alpha - \beta$  plane.

We thank the anonymous referee for valuable comments and suggestions, which allowed us to significantly improve the presentation of the paper. We acknowledge Kavli Institute for Astronomy and Astrophysics, Peking University, for hospitality where this research is carried out. BZ acknowledges a Cheung Kong Scholarship in China. This work is partially supported by NSF AST-0908362.

## REFERENCES

- Blandford, R. D., & McKee, C. F. 1976, *Physics of Fluids*, 19, 1130
- Chevalier, R. A., & Li, Z.-Y. 2000, *ApJ*, 536, 195
- Costa, E., Frontera, F., Heise, J., et al. 1997, *Nature*, 387, 783
- Curran, P. A., Evans, P. A., de Pasquale, M., Page, M. J., van der Horst, A. J. 2010, *ApJ*, 716, L135
- Dai, Z. G., & Cheng, K. S. 2001, *ApJ*, 558, L109
- Evans, P. A., Beardmore, A. P., Page, K. L., et al. 2009, *MNRAS*, 397, 1177
- Filgas, R., Greiner, J., Schady, P. et al. 2011, *A&A*, 535, A57
- Gao, H., Lei, W.-H., Zou, Y.-C., Wu, X.-F., Zhang, B. 2013, *New Astron. Rev.*, submitted
- Gehrels, N., Chincarini, G., Giommi, P., et al. 2004, *ApJ*, 611, 1005
- Granot, J., & Sari, R. 2002, *ApJ*, 568, 820
- Kobayashi, S., & Sari, R. 2000, *ApJ*, 542, 819
- Leventis, K., van Erten, H. J., Meliani, Z., Wijers, R. A. M. J. 2012, *MNRAS*, 427, 1329
- Liang, E.-W., Racusin, J. L., Zhang, B., Zhang, B.-B., & Burrows, D. N. 2008, *ApJ*, 675, 528
- Liang, E.-W., Zhang, B.-B., & Zhang, B. 2007, *ApJ*, 670, 565
- Mészáros, P., & Rees, M. J. 1997, *ApJ*, 476, 232
- Nousek, J. A., Kouveliotou, C., Grupe, D., et al. 2006, *ApJ*, 642, 389
- Oates, S. R., Page, M. J., Schady, P. et al. 2011, *MNRAS*, 412, 561
- Panaitescu, A. 2007, *MNRAS*, 379, 331
- Sari, R., Piran, T., & Halpern, J. P. 1999, *ApJ*, 519, L17
- Sari, R., Piran, T., & Narayan, R. 1998, *ApJ*, 497, L17+
- Uhm, Z. L. 2011, *ApJ*, 733, 86
- Uhm, Z. L., & Zhang, B. 2013, submitted (arXiv:1303.2704)

- Uhm, Z. L., Zhang, B., Hascoët, R., et al. 2012, *ApJ*, 761, 147 (U12)
- van Eerten, H. J., Wijers, R. A. M. J. 2009, *MNRAS*, 394, 2164
- van Paradijs, J., Groot, P. J., Galama, T., et al. 1997, *Nature*, 386, 686
- Willingale, R., O’Brien, P. T., Osborne, J. P., et al. 2007, *ApJ*, 662, 1093
- Zhang, B., Fan, Y. Z., Dyks, J., et al. 2006, *ApJ*, 642, 354
- Zhang, B., & Mészáros, P. 2004, *International Journal of Modern Physics A*, 19, 2385

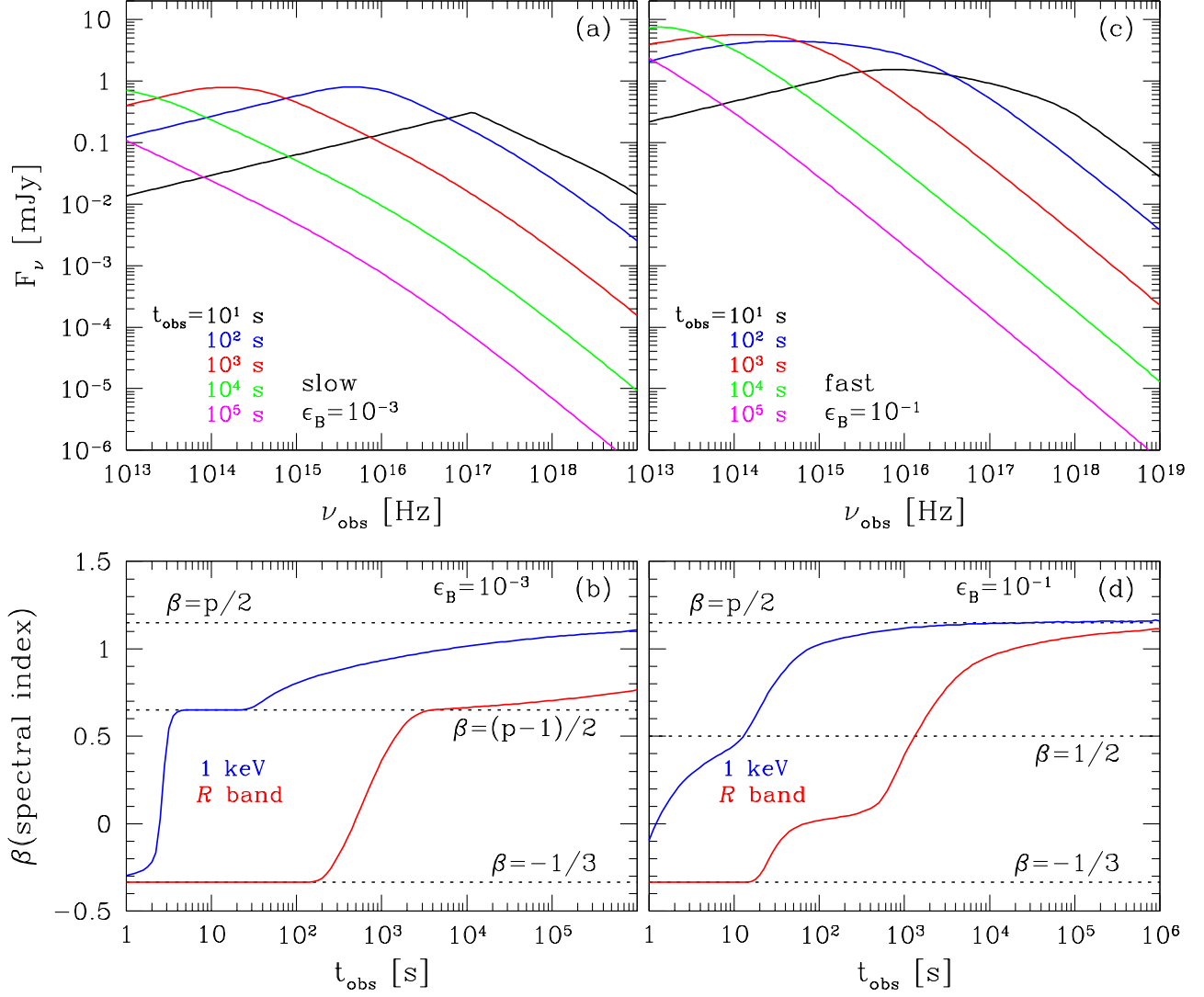


Fig. 1.— Afterglow spectra of the fiducial example at different observation times. A constant profile of pressure is adopted for the shocked blast region. Equation (1) is used to calculate the cooling history of electron energies. The curvature effect is also fully taken into account. Following parameters are adopted:  $L_{\text{ej}}(\tau) = L_0 = 10^{52}$  erg/s,  $\tau_b = 5$  s,  $E_b = 5 \times 10^{52}$  erg,  $n_1 = 1 \text{ cm}^{-3}$ ,  $\Gamma_{\text{ej}} = 300$ ,  $z = 1$ ,  $p = 2.3$ ,  $\epsilon_e = 0.1$ . *Top Left*: slow cooling case with  $\epsilon_B = 0.001$ . *Bottom Left*: spectral index  $\beta$  evolution as a function of observer time  $t_{\text{obs}}$  for the slow cooling case, which shows a very slow transition of  $\nu_c$  crossing. *Top Right*: fast cooling case with  $\epsilon_B = 0.1$ . *Bottom Right*:  $\beta$  evolution for the fast cooling case.

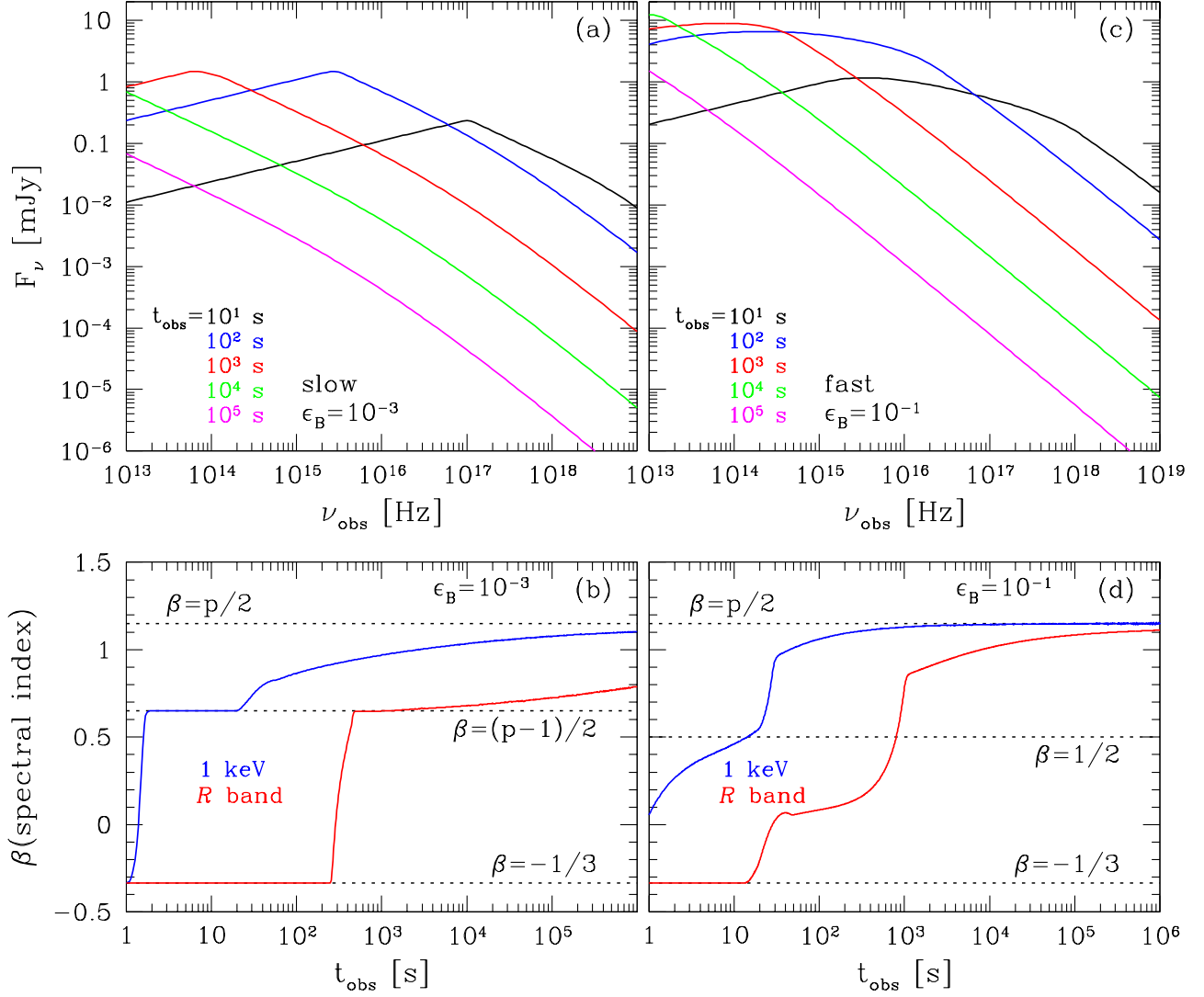


Fig. 2.— Calculation of the same problem as Figure 1, but without including the curvature effect to allow identification of the key physical origin of  $\nu_c$  smoothing. The notations of all 4 panels are the same as Figure 1.

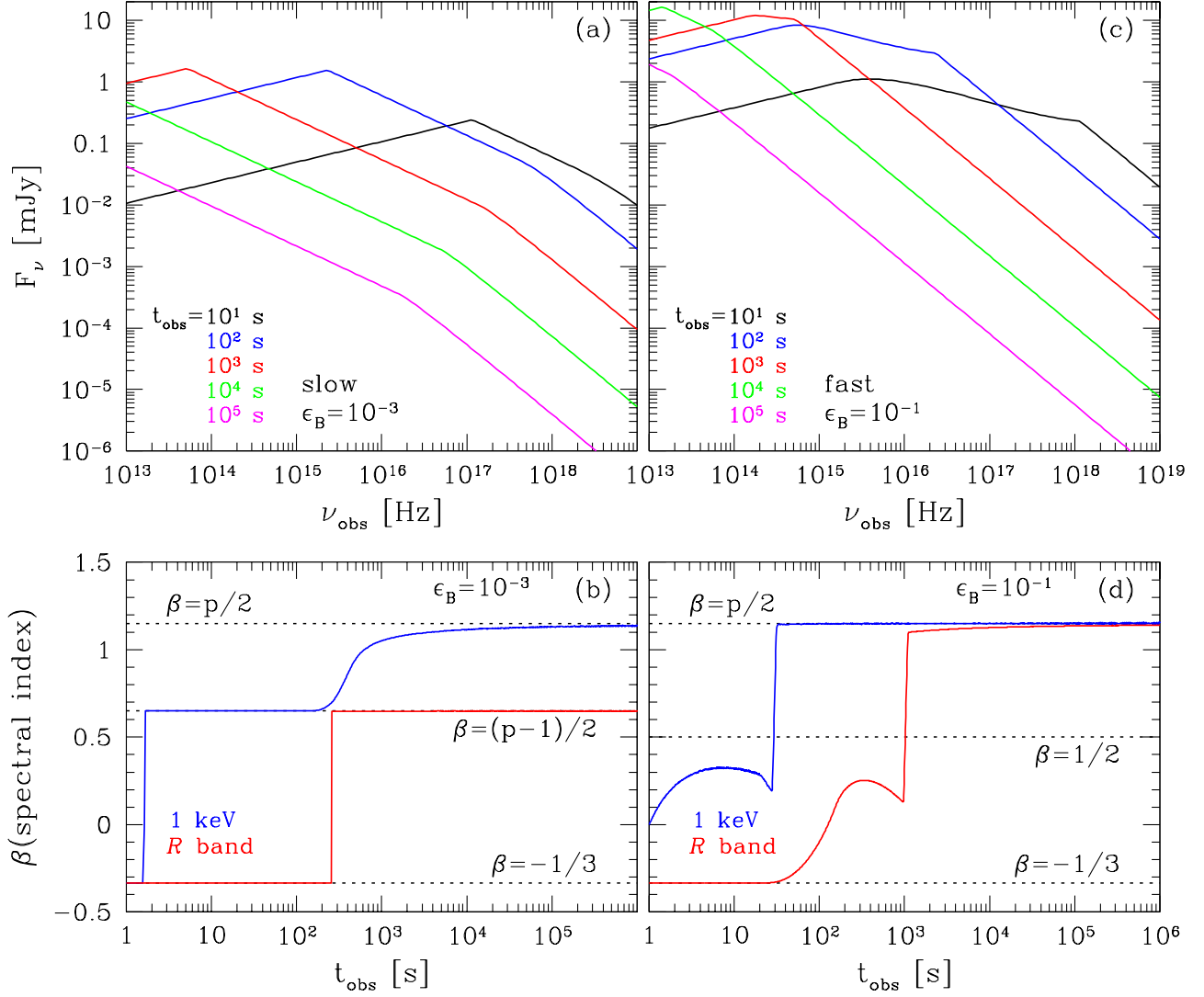


Fig. 3.— Calculation of the same problem as Figure 2, but with the simple, unjustified prescription as described in Equation (5). The notations of all 4 panels are the same as Figure 1. A sharp  $\nu_c$  is reproduced.

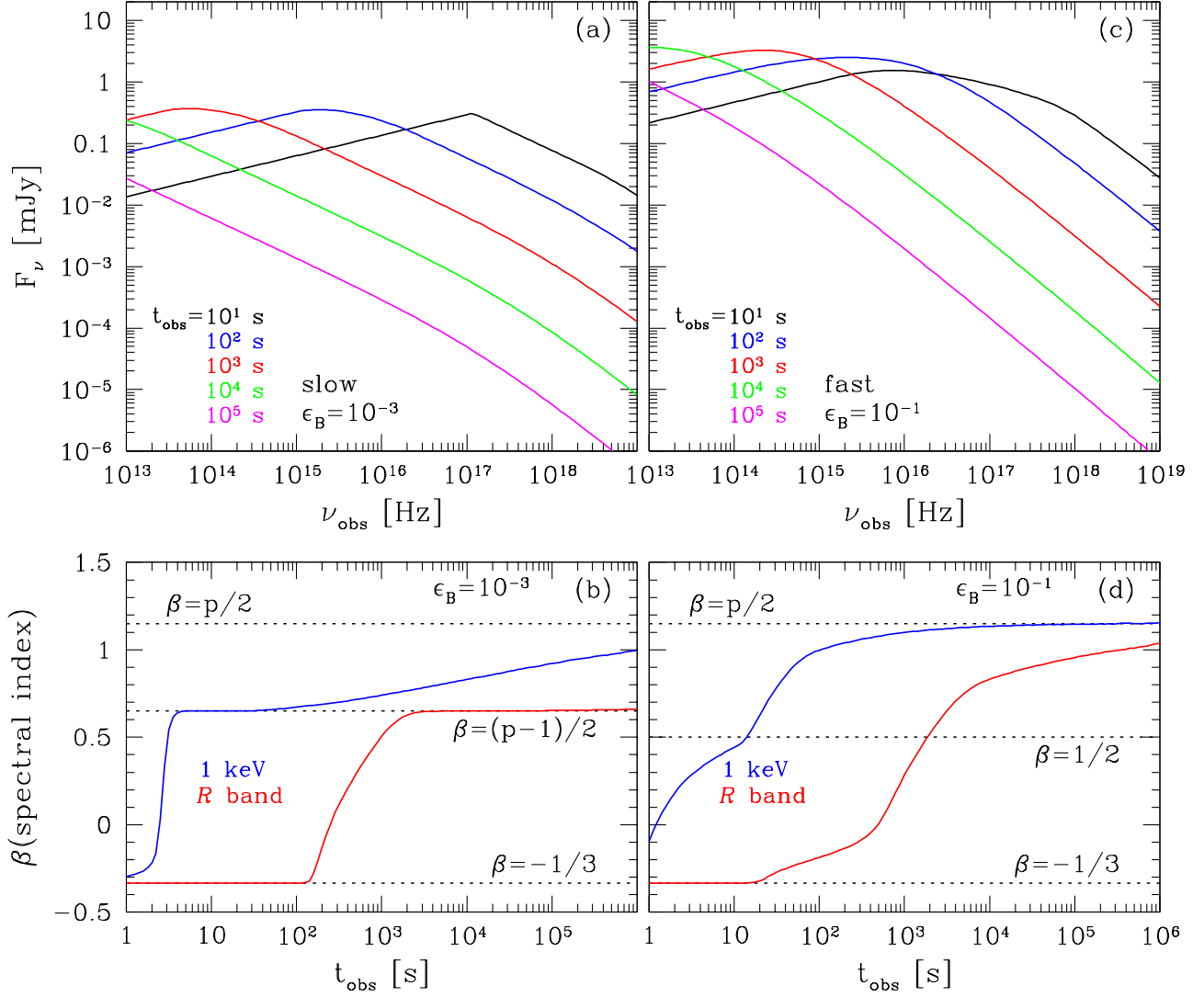


Fig. 4.— Calculation of the same problem as Figure 1, but with the BM profiles for the blast wave. The notations of all 4 panels are the same as Figure 1.



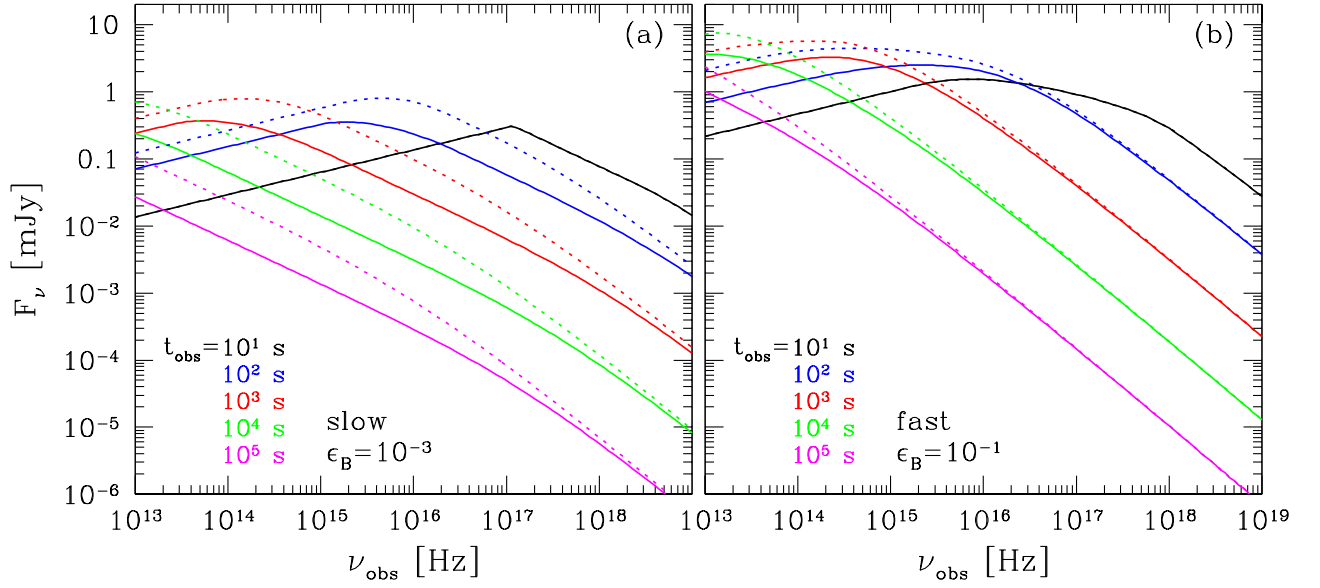


Fig. 5.— Comparison between two different profiles: solid line for spectra from Figure 4 (BM profile) and dotted line for spectra from Figure 1 (constant profile). *Left*:  $\epsilon_B = 0.001$  (slow cooling). *Right*:  $\epsilon_B = 0.1$  (fast cooling).